

NEAR-FIELD OPTICAL MICROSCOPY AND SPECTROSCOPY WITH POINTED PROBES*

Lukas Novotny¹ and Stephan J. Stranick²

¹*The Institute of Optics, University of Rochester, Rochester, New York 14627; email: novotny@optics.rochester.edu*

²*Surface and Microanalysis Science Division, National Institute of Standards and Technology, Gaithersburg, Maryland 20899; email: stranick@nist.gov*

Key Words scatter-probe, enhanced-probe, evanescent-probe

■ **Abstract** In recent years, developments in near-field techniques exploiting far-field illumination of a pointed, apertureless probe have demonstrated a newfound excitement. This is due in part to the advantages afforded by apertureless techniques that allow for the practical implementation of spectroscopic contrast mechanisms at length scales below 100 nm. These mechanisms include Raman and infrared absorption for chemical contrast, as well as materials contrast based on dielectric dispersion. In this review, we briefly describe the evolution of the field from the “classical” aperture-based approach toward the development of near-field optical microscopy with pointed probes. We highlight advances in state-of-the-art theory that describe the field distribution under an illuminated probe, as well as advances in the experimental implementation of scattering and excitation probe techniques.

INTRODUCTION

Progress in science and medicine is often triggered by new techniques and instrumentation. In the words of Nobel Laureate Rosalyn Yalow, “New Truths become evident when new tools become available.” Through the development and implementation of new microscopy and spectroscopy techniques, we have increased our understanding of physical phenomena ranging from the atomic structure of superconductors to the structure and function of living cells. These advances aside, numerous challenges remain. Often, the physical and chemical properties of nanometer-scale systems are studied by isolating specific components from their natural environment to employ standard/conventional spectroscopic techniques. For example, in nanotechnology one often attempts to understand the

*The U.S. Government has the right to retain a nonexclusive, royalty-free license in and to any copyright covering this paper.

Report Documentation Page

Form Approved
OMB No. 0704-0188

Public reporting burden for the collection of information is estimated to average 1 hour per response, including the time for reviewing instructions, searching existing data sources, gathering and maintaining the data needed, and completing and reviewing the collection of information. Send comments regarding this burden estimate or any other aspect of this collection of information, including suggestions for reducing this burden, to Washington Headquarters Services, Directorate for Information Operations and Reports, 1215 Jefferson Davis Highway, Suite 1204, Arlington VA 22202-4302. Respondents should be aware that notwithstanding any other provision of law, no person shall be subject to a penalty for failing to comply with a collection of information if it does not display a currently valid OMB control number.

1. REPORT DATE 2006		2. REPORT TYPE		3. DATES COVERED 00-00-2006 to 00-00-2006	
4. TITLE AND SUBTITLE Near-Field Optical Microscopy and Spectroscopy with Pointed Probes				5a. CONTRACT NUMBER	
				5b. GRANT NUMBER	
				5c. PROGRAM ELEMENT NUMBER	
6. AUTHOR(S)				5d. PROJECT NUMBER	
				5e. TASK NUMBER	
				5f. WORK UNIT NUMBER	
7. PERFORMING ORGANIZATION NAME(S) AND ADDRESS(ES) University of Rochester, The Institute of Optics, Rochester, NY, 14627				8. PERFORMING ORGANIZATION REPORT NUMBER	
9. SPONSORING/MONITORING AGENCY NAME(S) AND ADDRESS(ES)				10. SPONSOR/MONITOR'S ACRONYM(S)	
				11. SPONSOR/MONITOR'S REPORT NUMBER(S)	
12. DISTRIBUTION/AVAILABILITY STATEMENT Approved for public release; distribution unlimited					
13. SUPPLEMENTARY NOTES					
14. ABSTRACT see report					
15. SUBJECT TERMS					
16. SECURITY CLASSIFICATION OF:			17. LIMITATION OF ABSTRACT	18. NUMBER OF PAGES	19a. NAME OF RESPONSIBLE PERSON
a. REPORT unclassified	b. ABSTRACT unclassified	c. THIS PAGE unclassified			

nanometer-scale building blocks in an isolated form before assembling them into a functional device. However, the properties of the building blocks can change once they are embedded into a macroscopic structure. This change is due to interactions between the building blocks and their environment. Interestingly, many nanometer-scale biological systems function only in their native environment. For example, the specific function of certain membrane proteins depends on the presence of other neighboring proteins (e.g., energy transfer between light-harvesting complexes in photosynthetic membranes). Thus, the challenge is to develop tools that perform measurements on complex, heterogeneous nanometer-scale systems with the same exacting level of chemical and physical detail that conventional microscopic and spectroscopic techniques currently provide on macroscopic sample systems.

Common high-resolution instruments for the characterization of surfaces include electron microscopy and scanning-probe microscopy. Recent experiments have demonstrated the ability of these techniques to image and manipulate materials ranging from individual atoms to proteins. However, without any prior knowledge about the specimen, it is often difficult or challenging to identify the constituent parts. This challenge is mainly a result of the fact that electron microscopy and most scanning-probe microscopies render high-resolution topographic images with little or no chemical information. The lack of chemical information is related to the particular molecular structure and composition of the sample. The chemical information can, however, be retrieved from probing the bond energies between adjacent atoms.

Optical spectroscopy provides a wealth of information on structural and dynamical properties of materials. This is because the energies of light quanta (photons) lie in the energy range of electronic and vibrational transitions in matter. Combining optical spectroscopy with microscopy is especially desirable because spectral features can then be spatially resolved. However, the diffraction limit has prevented researchers from resolving features smaller than half a wavelength of the applied radiation. Two decades ago, it was demonstrated that near-field optical microscopy (1, 2) was able to extend the range of optical measurements beyond the diffraction limit. Although the attainable spatial resolution does not presently compare to related scanning-probe techniques (e.g., scanning-tunneling microscopy), it is the combination of resolution and chemical information that makes near-field optical microscopy attractive (see Figure 1).

Over the past 10 years, developments in near-field optical microscopy have been summarized in several review articles and books (3–10). Our intention is not to provide another wide-spanning review of near-field optical microscopy but to describe a relatively new trend based on laser-irradiated pointed probes. Here, we briefly describe the “classical” aperture-based approach and give a rough historical account of the development and application of near-field optical microscopy and spectroscopy with pointed probes often referred to as apertureless probes.

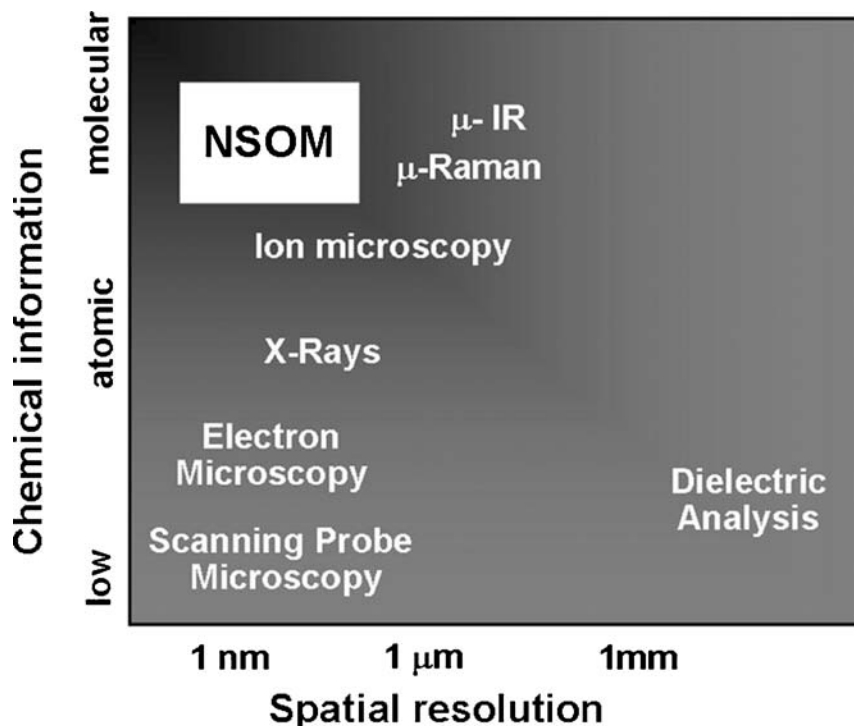


Figure 1 Chemical specificity versus spatial resolution for different microscopic techniques. Near-field scanning optical microscopy (NSOM) achieves an excellent product of the two factors.

APERTURE-BASED NEAR-FIELD OPTICAL MICROSCOPY

As illustrated in Figure 2, the spatial resolution Δx of standard optical microscopy is limited by diffraction to roughly (Abbé criterion)

$$\Delta x = 0.61\lambda/NA.$$

Here, λ is the wavelength of the interacting radiation, and $NA = n \sin \alpha$ is the numerical aperture of the objective lens. The NA can be increased by a large index of refraction n of the surrounding medium or a large angle of acceptance α . The latter two tricks are routinely applied in confocal microscopy (e.g., solid immersion-lens microscopy and 4π -microscopy). By using prior information about the sample properties (e.g., the energy-level structure of dye molecules) or by applying non-linear or saturation effects (e.g., multiphoton-confocal microscopy and stimulated depletion), it is possible to stretch the Abbé resolution criterion further.

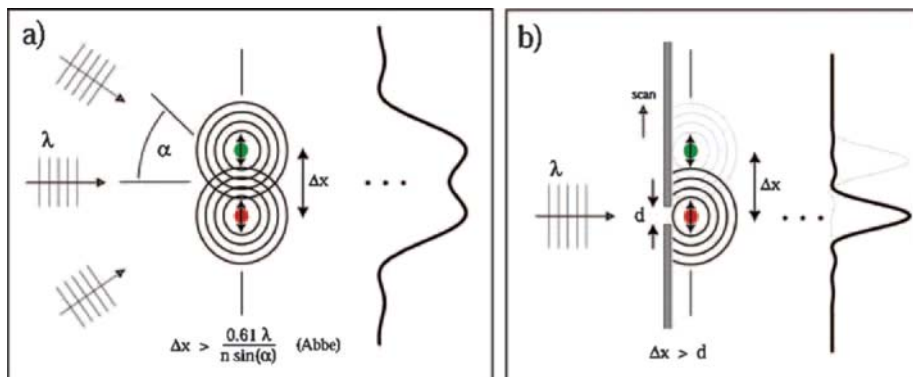


Figure 2 Comparison of diffraction-limited optical microscopy and near-field optical microscopy. (a) Schematic representation of the diffraction limit showing the minimum detectable separation of two light scatterers. (b) Schematic of aperture scanning near-field optical microscopy. To first approximation, resolution is defined by the aperture size and not by the wavelength of the exciting radiation.

In near-field optical microscopy, the resolution Δx no longer depends on λ but on a characteristic length d (e.g., aperture diameter or tip diameter) of a local probe. Near-field optical microscopy relies on a confined photon flux between a local probe and the sample surface. The probe is raster-scanned over the sample surface, and for predefined positions (x, y) of the probe, a remote detector acquires the optical response. In this way an optical contrast image can be recorded. In Syngé's original concept, the local probe consisted of a tiny aperture in a perfectly reflecting metal screen (11) (see Figure 2b). Immediately behind the irradiated screen, the light field is spatially confined to the size of the aperture (d). Only if a scatterer is within a distance d from the aperture will it interact with the radiation field. Syngé's idea was soon forgotten after its inception because nanofabrication techniques were not then available. In the following decades, however, the idea was reinvented several times. The first experimental results performed at optical frequencies were published by Pohl et al. at the IBM Research Laboratory in Switzerland followed shortly by Lewis et al. at Cornell University (1, 2). A reproduction of the first near-field optical measurement is shown in Figure 3.

In the most widely adapted aperture approach, light is sent down an aluminum-coated fiber tip of which the foremost end is left uncoated to form a small aperture (12). Unfortunately, only a tiny fraction of the light coupled into the fiber is emitted through the aperture because of the propagation cutoff of the waveguide modes (13). The low-light throughput and the finite skin depth of the metal are the limiting factors for resolution. The throughput can be significantly increased by using probes with large cone angles (13, 14). Nevertheless, it is doubtful that a reproducible artifact-free resolution of 50 nm will be surpassed by the current aperture technique. Moreover, the aperture technique has other practical complications

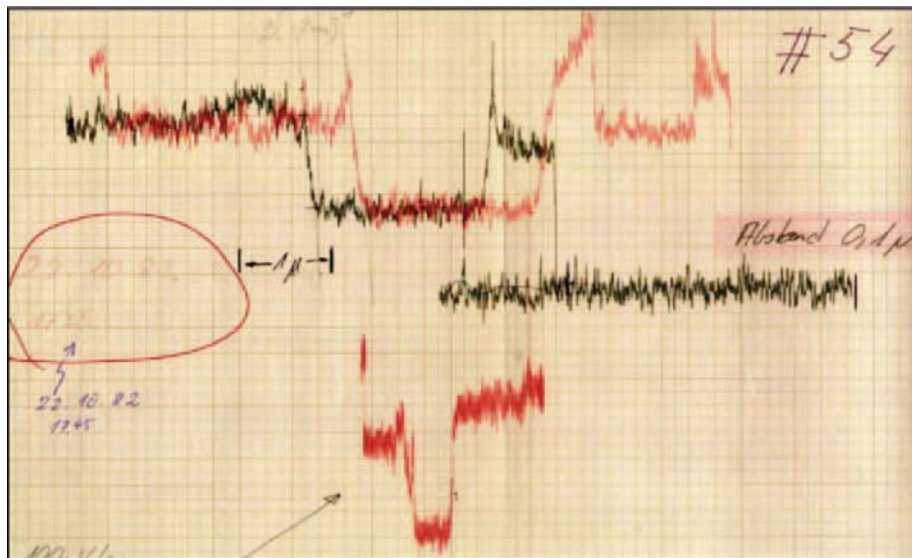


Figure 3 Early near-field optical scan trace recorded with an aperture-type probe. The data are from the laboratory book of Winfried Denk, then working with Dieter W. Pohl at the IBM Research Laboratory in Switzerland. (Figure courtesy of Dieter W. Pohl)

including the following: The difficulty in obtaining a smooth aluminum coating introduces nonreproducibility in probe fabrication, the flat ends of the aperture probes are not suitable for simultaneous topographic imaging with high resolution, and the absorption of light in the metal coating causes significant heating that poses a problem for temperature-sensitive applications (15, 16). These issues limit the aperture technique's impact in key technologies and nanoscience applications.

NEAR-FIELD OPTICAL MICROSCOPY WITH POINTED PROBES

Laser-irradiated pointed probes were introduced to overcome the limitations of aperture probes and to improve the resolution in near-field optical microscopy (17–25). Two different schemes were established: the local-scattering approach and the local-excitation approach. In the local-scattering approach, a pointed probe such as a tip or a particle is used to locally perturb the fields at a sample surface; the response to this perturbation is detected in the far field at the same frequency of the incident light. This scheme relies on the fact that the field near any laser-irradiated object is made of waves that propagate away from the object (propagating waves) and also of waves that remain attached to the object's surface (evanescent waves). The inability of evanescent waves to propagate constitutes the diffraction limit

of classical microscopy. However, they can be partially converted to propagating radiation by using a pointed probe as a local scatterer. Scattering-type measurements typically have a high signal-to-noise ratio, but the interpretation of the recorded information is complicated by so-called topographic artifacts (26). The problem is related to the fact that the scattering efficiency depends sensitively on the separation between probe and sample, making the differentiation of true optical contrast (related to local-dielectric constant) difficult. Nevertheless, schemes have been worked out to largely decouple optical and topographic information. These schemes are discussed in more detail in the section on scattering-type near-field microscopy below.

Instead of using the pointed probe as a local scatterer, one can use it as a local light source. This is accomplished under the proper polarization and excitation conditions through the use of suitable probe materials and probe geometries (27, 28). Under these conditions, the field near the apex of the probe can become strongly enhanced over the field of the illuminating laser light, thereby establishing a nanoscopic light source. Thus, instead of using a tip to locally scatter a sample's near field, one can use the tip to provide a local-excitation source for a spectroscopic response of the sample (23, 24). As shown in Figure 4 the tip is held a few nanometers above the sample surface so that a highly localized interaction between the enhanced field and the sample is achieved. This approach enables simultaneous spectral and sub-diffraction spatial measurements, but it depends sensitively on the magnitude of the field-enhancement factor. The local-excitation scheme is commonly referred to as tip-enhanced near-field optical microscopy, and it is

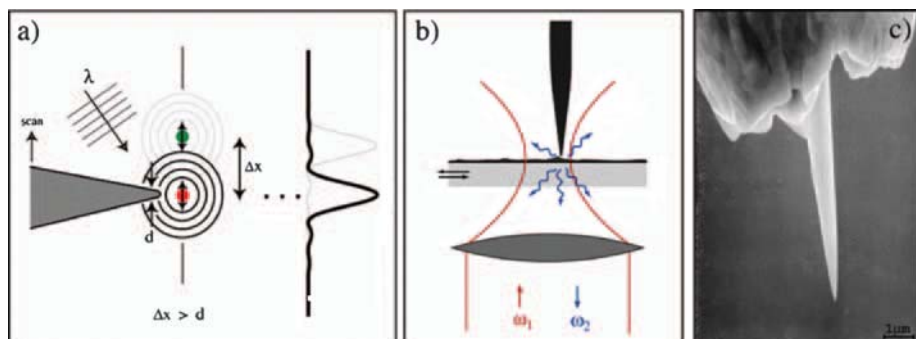


Figure 4 Principle of tip-enhanced near-field optical microscopy. A laser-irradiated metal tip (polarization along tip axis) enhances the incident electric field near its apex thereby creating a localized photon source. (a) Schematic of the method. (b) Practical implementation: A higher-order laser beam is focused on a sample surface, and a sharply pointed metal tip is positioned into the laser focus. The enhanced fields at the tip locally interact with the sample surface thereby exciting a spectroscopic response collected by the same objective and directed on a detector. (c) Scanning electron microscopy image of a sharp gold tip fabricated by focused-ion beam milling.

discussed in more detail in the section on local excitation below. In principle, the two methods, local excitation and local scattering, are not independent. A strong field enhancement is a necessary condition for efficient scattering and vice versa.

DEVELOPMENT OF NEAR-FIELD OPTICAL MICROSCOPY WITH POINTED PROBES

The use of a light-irradiated particle for achieving subwavelength light localization was originally suggested by Synge in a letter to Einstein (29). The idea was never published in its original form because there was concern that the direct exposure of the sample to the irradiating light would overshadow the local interaction between particle and sample. Instead in 1928, Synge (11) published an article in which he proposed the use of a tiny aperture in a metal screen to achieve a subwavelength-scale light source (see the section on the aperture technique above). In 1984, even before the invention of the atomic force microscope (AFM), Wessel (30) proposed a concept similar to Synge's original idea: A laser-irradiated, elongated metal particle is used to establish an enhanced, localized light field. Wessel's proposal was soon forgotten, but it resurfaced again in the context of near-field optical microscopy. In fact, within this field of study several research groups reinvented Wessel's idea. Denk & Pohl (22) suggested using the enhanced field at a metal tip in combination with nonlinear-optical spectroscopy, and Fischer & Pohl (31) produced the first experimental results demonstrating the field-enhancement effect associated with a single metal nanoparticle. In the following years, metal tips were introduced as scattering centers to convert the nonpropagating evanescent fields near the surface of an object into propagating radiation. This was the initial approach taken by Inouye & Kawata (17). In their paper they speculate about a combination of metal tips with surface-enhanced spectroscopy. Similar scattering-type approaches were pursued by the groups of Boccarda (32) and Wickramasinghe (18). The latter implemented an interferometric detection scheme for the locally perturbed near field. However, the origin of the contrast in the recorded images was long debated. Keilmann and coworkers (20, 21) pursued a parallel effort in scattering-type near-field microscopy with experiments performed at radio frequencies and later in the infrared. Recently, this group has established the possibility of extracting various optical parameters using a pointed probe as a local scatterer (33, 34).

Although local-scattering near-field optical microscopy has found important applications in materials science, it is not inherently a spectroscopic technique. The use of the field-enhancement effect near a metal tip for localized spectroscopic measurements was theoretically formulated in Reference 23 and subsequently experimentally demonstrated by Sanchez et al. (24) using two-photon excited fluorescence. This approach was inspired by the field distribution near a tiny aperture as shown in Figure 5a. The field is dominated by two strong lobes near the rims of the aperture. These lobes are located in the direction of the incident polarization and originate from surface charges accumulating at the rims. As shown in Figure 5,

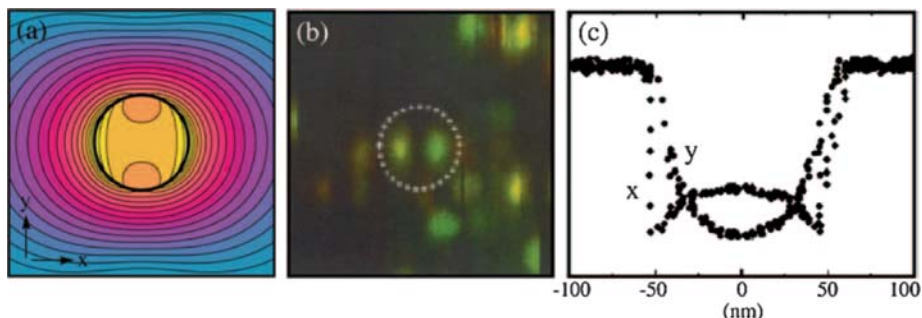


Figure 5 Early evidence of field enhancement at the rims of an aperture. (a) Intensity distribution (E^2) in a plane 1 nm in front of the end-face of an aperture probe. The circle indicates the physical boundary between the dielectric fiber core and the aluminum coating. Factor of $2^{1/2}$ between adjacent contour lines. From Reference 13. (b) Fluorescence image of single molecules imaged with an aperture probe. The pattern inside the circle results from a molecule oriented perpendicular to the aperture plane. It is excited only by the enhanced field at the rims of the aperture. From Reference 37. (c) Scattering intensity recorded by scanning an aperture probe over a thin AlAs layer sandwiched between two GaAs half spaces. The figure shows the traces along the two major directions labeled x and y in part a. From Reference 35.

these lobes were experimentally verified by scanning the aperture over a sharp line (35) and by using single molecules as local probes (36, 37).

Because of the enhanced fields at the aperture rims, the field confinement cannot be better than the physical size of the aperture diameter. It is evident that much better confinement would result if the metal rim was reduced to a single point as in the case of a metal tip. Earlier theoretical studies by Denk & Pohl (22) demonstrated that the quasi-static fields in the gap between a tip and a substrate can be extremely strong and that this effect can be instrumental for inelastic tunneling and light emission during scanning-tunneling microscopy. Later, researchers theoretically established that the field-enhancement effect must be driven by an external field polarized along the axis of the pointed probe (27, 28). Interestingly, the field enhancement was also studied in the context of scanning-tunneling microscopy as it was believed to mediate the transfer of atoms from the tip to the sample (38–40). Following these experiments, the local-excitation method based on a laser-irradiated metal tip was extended to other spectroscopic interactions such as Raman scattering (25, 41–43) and coherent anti-Stokes Raman scattering (CARS) (44). In essence, the original ideas of Syngé and Wessel have made their way into real applications.

In the following sections, we describe in more detail near-field optical microscopy based on pointed probes. We first review theoretical work aimed at understanding the field-enhancement effect and the associated electromagnetic-field distributions. Next, we concentrate on the local-scattering approach in which a pointed probe is used to locally scatter the evanescent fields near an irradiated

object. We then turn our attention to the local-excitation scheme where the field enhancement at pointed probes is explicitly used as a local light source. Finally, we provide a short summary and discuss possible future trends.

FIELD DISTRIBUTION NEAR POINTED PROBES

In this section, we discuss the electromagnetic-field distribution near laser-irradiated pointed probes and concentrate on metal particles and tips. Although various experimental studies using dielectric or semiconducting tips have demonstrated the capability of performing nanoscale imaging (45–48), it is generally accepted that the field enhancement and the scattering efficiency are stronger for metal tips (23, 24, 28, 49, 50). At optical frequencies, metals are characterized by a small skin depth and by electromagnetic resonances associated with the free electrons in the metal. Depending on the type of the metal and its geometry, the collective response of the free electrons can greatly enhance the electric-field strength of the incoming radiation. The coupled excitation of electrons and electromagnetic field is generally referred to as a surface plasmon, although, by definition, the term denotes the quantum of surface-charge-density oscillations. Because the surface-charge oscillations are intimately coupled to electromagnetic fields, surface plasmons are polaritons.

In the context of near-field optical microscopy, pointed metal probes are used in localizing and enhancing optical radiation (see Figure 4). In principle, these probes fulfill the role of standard optical lenses used in imaging. However, in this context they no longer work as linear elements and are no longer limited by the laws of diffraction. Their function is similar to electromagnetic antennas that convert propagating radiation into a confined zone called the feedgap. In the feedgap, electric circuitry either releases or receives the signal associated with the electromagnetic field. Because of this similarity, pointed metal probes used in near-field optics are also referred to as optical antennas. The challenge in the design of an antenna is to efficiently match the impedances of the near zone and the far zone of the source (or receiver). In other words, the antenna locally modifies the density of electromagnetic states, thereby increasing the modes into which the source can radiate and vice versa. The most efficient antenna designs implemented at optical frequencies are the lambda-half antenna (51) and the bow-tie antenna (52–54). However, by making use of electromagnetic resonances associated with surface plasmons, any metal nanostructure can be viewed as an optical antenna. Of course, the efficiency depends on the material composition and the geometry of the nanostructure.

A simple form of optical antenna is a single ellipsoidal particle. This particle exhibits a distinct resonance for which the field enhancement at the poles and the scattering efficiency is maximized (55). It has been determined both theoretically and experimentally that the sharpness of the resonance, as determined by the radiative decay of surface plasmons, depends strongly on particle size and shape (56–59).

Silver and gold particles can be grown in various shapes (60–62), and the spectral position of plasmon resonances can be measured by dark-field microscopy using a broadband excitation source. Spherical gold particles have been attached to the end of fiber tips and used as near-field optical probes (63). Although ellipsoidal particles have superior properties, they have not been used because of difficulties in attaching them in a preferred orientation. However, it can be expected that these technical challenges will be overcome soon, for example, by using electrostatic gradient forces generated by a potential applied between tip and a counter electrode (27).

It is also important to notice that the quality of the resonance depends on the excitation conditions. For example, if the particle is excited by an evanescent wave, the symmetry is broken and the resonance splits into two peaks (64). The same results occur if the particle is placed in an inhomogeneous environment, such as close to a metal interface. Generally, one of the resulting resonances dominates the optical properties. A long ellipsoidal particle of which only one pole is irradiated is the equivalent of a tip. Besides apertures, metal tips are the most commonly used probes in near-field optical microscopy. They are easy to fabricate and manipulate. The field enhancement at a sharp tip arises from a combination of a quasi-static lightning-rod effect and surface-plasmon excitations (27). The former is a result of the near singularity at the tip; because Maxwell's equations are second-order differential equations, the fields can become singular when the first or second derivative is not defined. However, real metals have finite conductivity, and the radius of curvature at the tip is finite. Consequently, there is no real field singularity, but the field at the tip can be strongly enhanced. The surface-plasmon excitation stems from resonances in the collective electron oscillations. However, because of the open geometry, one does not expect a pronounced resonance as in the case of a finite, ellipsoidal particle (65).

A tip is a challenging geometry, and one is forced to use numerical methods to analyze the field distributions resulting from a particular external irradiation. Several studies have been performed using different tip geometries, tip materials, and excitation conditions (23, 27, 28, 56, 57, 66–68). As an example, Figure 6 shows the calculated field distribution resulting from plane-wave excitation of a gold tip at a wavelength of $\lambda = 650$ nm.

Figure 7 shows the calculated surface-charge density on a gold tip when the tip is excited by a wave polarized along the tip axis. The surface charge oscillates with the same frequency as the exciting field. Close to the tip apex, the induced surface-charge density is rotationally symmetric and has the highest amplitude at the end of the tip. The surface charges form an oscillating standing wave with wavelengths shorter than the wavelength of the illuminating light (27). On the other hand, when the polarization is perpendicular to the tip axis (not shown), the tip is simply polarized in the transverse plane and there is no surface-charge accumulation at the tip.

A factor not considered in most theoretical investigations is the loss as a result of nonlocal effects. In bulk materials electrons lose their kinetic energy as a result of scattering at the lattice. However, when the size of the tip becomes comparable with

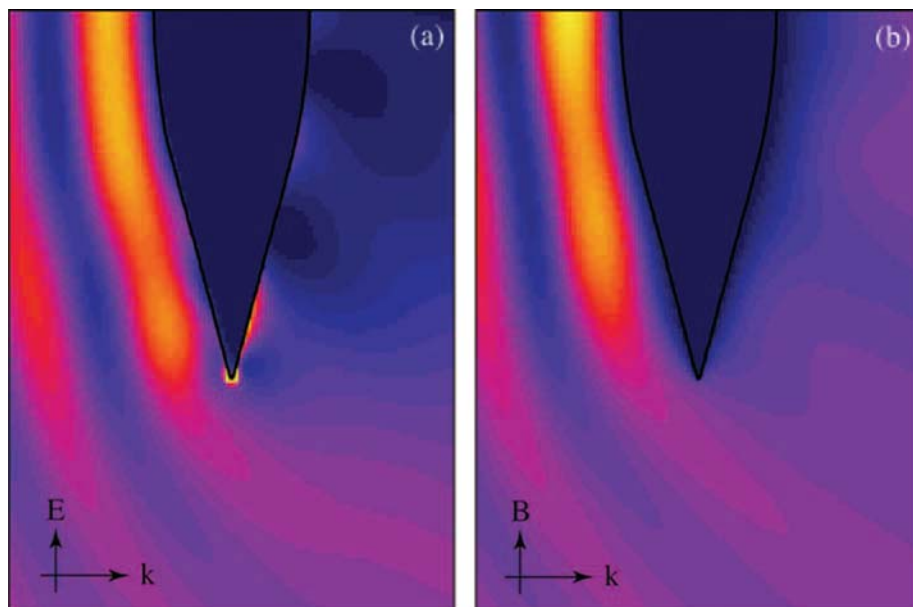


Figure 6 Calculated intensity distribution near a laser-irradiated gold tip. The exciting wave is incident from the left and forms a standing wave pattern as it interferes with the reflected field from the tip shaft, and at the end of the tip, the wave diffracts. Two different excitation polarizations are used. The field-enhancement effect is observed only if the incident wave is polarized along the tip axis (*a*). In the case of an incident wave polarized perpendicular to the tip axis, the field near the tip is attenuated (*b*).

the mean free path of the electrons, there is an increased probability that electrons also scatter at the interfaces. This scattering leads to increased dissipation and thus to additional damping of the field strength (imaginary part of dielectric constant increases) (69). These nonlocal effects can be taken into account in a theoretical analysis (70, 71), but it is not possible to derive quantitative results because the nonlocal parameters are simply not known.

To gain a more physically intuitive understanding for the optical response of a metal tip, it is favorable to find an approximate model that can be treated analytically. The simplest model for the tip is a quasi-static sphere. As shown in Figure 8, the sphere model is a good approximation if an anisotropic polarizability tensor α is used (72). According to this model (see Figure 7*b*), the external field \mathbf{E}_0 oscillating at the angular frequency ω induces a dipole \mathbf{p} in the tip according to

$$\mathbf{p}(\omega) = \begin{bmatrix} \alpha_{\perp} & 0 & 0 \\ 0 & \alpha_{\perp} & 0 \\ 0 & 0 & \alpha_{\parallel} \end{bmatrix} \mathbf{E}_0(\omega),$$

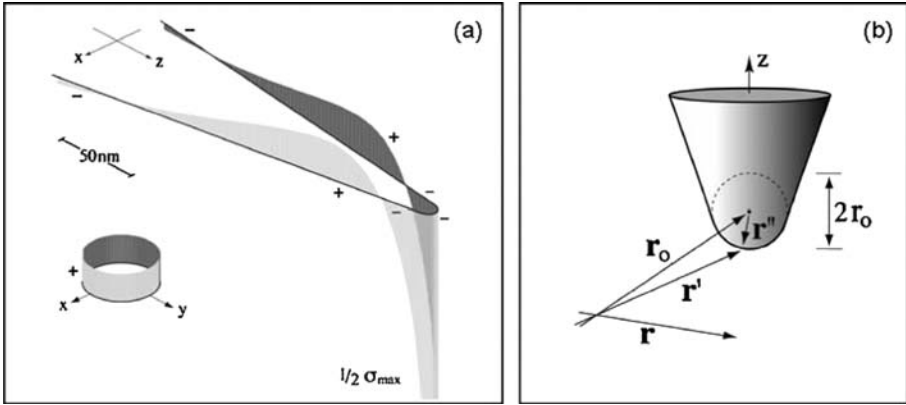


Figure 7 (a) Induced surface-charge density on the surface of a laser-irradiated gold tip captured at a certain instance of time. Polarization along the tip axis gives rise to a large surface-charge accumulation at the tip’s apex. The solid line indicates the tip geometry, whereas the shaded areas represent the surface charge. From Reference 27. (b) Coordinates used for the dipole model.

where we chose the z -axis to coincide with the tip axis. The transverse polarizability α_{\perp} is identical to the quasi-static polarizability of a small sphere

$$\alpha_{\perp}(\omega) = 4\pi\epsilon_0 r_o^3 \frac{\epsilon(\omega) - 1}{\epsilon(\omega) + 2},$$

where r_o is the tip radius, and ϵ is the dielectric function of the tip material. On the other hand, the longitudinal polarizability α_{\parallel} is given by

$$\alpha_{\parallel}(\omega) = 8\pi\epsilon_0 r_o^3 f_e(\omega),$$

where f_e is the complex field-enhancement factor. For a wavelength of $\lambda = 830$ nm, a gold tip with $\epsilon = -24.9 + 1.57i$, and a tip radius of $r_o = 10$ nm, our numerical calculations based on the multiple multipole method (73) lead to $f_e = -2.9 + 11.8i$. The expression for α_{\parallel} originates from the requirement that the magnitude of the field produced by $\mathbf{p}(\omega)$ at the surface of the tip is equal to the computationally determined field that we set equal to $f_e \mathbf{E}_o$. The electric field \mathbf{E} in the vicinity of the tip is now approximated as

$$\mathbf{E}(\mathbf{r}, \omega) = \mathbf{E}_o(\mathbf{r}, \omega) + \frac{1}{\epsilon_0} \frac{\omega^2}{c^2} \overset{\leftrightarrow}{\mathbf{G}}^o(\mathbf{r}, \mathbf{r}_o, \omega) \mathbf{p}(\omega),$$

where \mathbf{r}_o specifies the origin of \mathbf{p} , and $\overset{\leftrightarrow}{\mathbf{G}}^o$ is the free space dyadic Green’s function. The tip radius defines how close the dipole can be brought to a sample surface and how strong the field localization is. Because the external illumination \mathbf{E}_o not only excites the metal tip but also irradiates the sample surface, the field enhancement

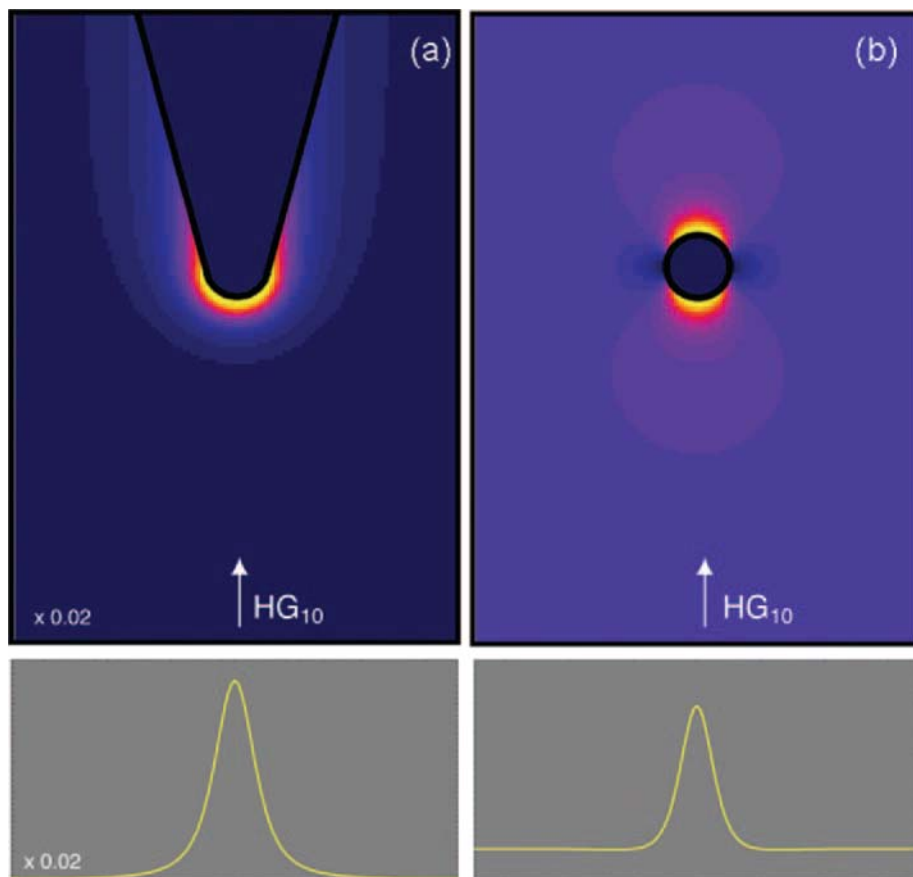


Figure 8 Comparison of field distributions (E^2) near a gold tip and a gold particle irradiated by an on-axis focused Hermite-Gaussian (1, 0) laser mode. At the apex of tip the exciting-laser field is polarized along the tip axis resulting in a longitudinal polarization. The resulting field is enhanced near the tip apex. The line scans at the bottom represent the field distribution on a transverse line 1 nm in front of tip and particle, respectively. However, the field distribution in the case of the metal tip has been scaled by a factor of 0.02. The qualitative agreement between the field distributions indicates that the tip can be modeled as a particle with a polarizability that depends on the field-enhancement factor.

needs to be strong enough to suppress the signal associated with direct sample irradiation.

Noble metals such as gold and silver are highly nonlinear materials that give rise to higher harmonic generation and luminescence when irradiated with laser pulses with high peak intensity. Nonlinear-signal generation at the apex of a bare metal tip provides ultrahigh-field localization that is basically background free and suitable for ultrahigh-resolution imaging (72, 74, 75). By using nonlinear susceptibilities

to describe the nonlinear-tip response, the dipole model can be easily extended to the nonlinear regime (72).

Above we consider a bare metal tip in free space. However, the presence of a sample surface will modify the field distribution and hence the field-enhancement factor. It is straightforward to apply established numerical techniques to study the influence of a sample surface. On the other hand, as stated above, an intuitive simple model is more useful in understanding the physical details.

The dipole model for the tip can be easily extended to account for the presence of a plane substrate by taking into account the image dipole. Because of the small size of the tip and the close proximity to the sample surface, the local field distribution can be considered in the quasi-static limit; i.e., all the fields in the region of interest oscillate in phase and retardation is ignored. In this limit, Helmholtz's equation reduces to Laplace's equation, which is readily solved by the method of images. Consequently, the field above the sample surface can be written as a superposition of the fields of two dipoles: (a) the field of a tip dipole and (b) the field of the image dipole located at a distance $d + r_o$ below the sample surface, d and r_o being the tip radius and tip-sample distance, respectively. It is possible to incorporate the influence of the image field into an "effective polarizability" according to

$$\mathbf{p} = \alpha[\mathbf{E}_o + \mathbf{E}_{\text{image}}] \equiv \alpha_{\text{eff}}\mathbf{E}_o.$$

Thus, the modification of the local field is equivalent to a modification of the tip's polarizability. It turns out that the magnitude of the image dipole depends on the orientation of the tip dipole. For the longitudinal component of the field (electric field in direction of tip axis) one obtains

$$\alpha_{\text{eff},\parallel} = \frac{\alpha_{\parallel}[1 + \beta]}{1 - \alpha_{\parallel}\beta/[16\pi\epsilon_o(d + r_o)^3]}, \quad 1$$

where β represents the quasi-static Fresnel-reflection coefficient defined as

$$\beta = \frac{\epsilon_{\text{sample}} - 1}{\epsilon_{\text{sample}} + 1}.$$

Here, ϵ_{sample} is the local-dielectric function of the sample. Similarly, for the transverse component (electric field parallel to sample surface) the effective polarizability is calculated as

$$\alpha_{\text{eff},\perp} = \frac{\alpha_{\perp}[1 - \beta]}{1 - \alpha_{\perp}\beta/[32\pi\epsilon_o(d + r_o)^3]},$$

which is different from the expression for the longitudinal part.

The scattering efficiency of the tip depends on the magnitude of the tip dipole and hence on the effective polarizability. Therefore, the scattered light bears information on tip-sample distance (d), the properties of the tip (a), and the properties of the sample (b). By keeping d and a constant, variations in scattered intensity as the tip is scanned over the sample surface can be ascribed to local changes in the

dielectric constant of the sample ϵ_{sample} . This spectroscopic capability has been demonstrated by Keilmann, Hillenbrand, and coworkers (33, 76, 77), and their results are discussed in the section on scattering-based approaches.

It has to be emphasized that the field enhancement and the scattering efficiency are interrelated phenomena. Hence, a near-field optical microscope working efficiently in local-excitation mode also works efficiently in the local-scattering mode. Finding conditions for a strong local-field enhancement benefits both measurement modalities.

SCATTERING-BASED APPROACHES

As outlined above, the local-scattering approach in near-field scanning microscopy takes advantage of the nonpropagating evanescent waves present at an irradiated sample's surface by using a pointed probe to locally perturb (scatter) these fields into radiation. In this approach, the primary measurable is the field scattered at the apex of the probe and generally at the same wavelength of the incident light. Given this, an increase in experimental complexity over standard near-field scanning microscopy (NSOM) schemes is required to detect and distinguish between the locally scattered fields from under the tip (near fields) and the background (far-field) light. The strength of the scattering is dependent on the electromagnetic interaction between the tip and the sample surface. These interactions are governed by the sample's local-dielectric constant, the probe's electromagnetic properties, and the probe-sample separation (78). Whereas the nature of the sample system varies, one aspect of the experimental system that remains nominally constant is the tip material. As discussed in the next section, noble metals such as gold provide excellent scattering efficiencies (17) and the potential for enhanced fields (79), but useable tips can be fabricated from dielectric and semiconducting materials as well (80, 81).

It is useful and instructive to look at some of the common aspects associated with scattering NSOM. The basic experimental configuration of the scattering near-field scanning optical microscope is shown in Figure 9. The AFM provides a means of maintaining the local scatterer (a metal-coated tip) in the near field of the surface: A practical definition of the near field is the region within a probe diameter of the sample surface. As the probe is raster-scanned over the surface, the tapping-mode feedback scheme maintains a constant average gap. This allows one to acquire the topography of the surface while simultaneously recording its optical response. Unlike in a conventional tapping-mode AFM, the tapping-mode amplitude (tip-sample separation) is normally set to a value on the order of the spatial extent of the near field. A fast lens is used to collect the scattered light, which is comprised of locally scattered light as well as background scattering from the extended structures of the tip and sample. The local near-field scattering is discriminated from the background scattering using lock-in detection at the tapping-mode frequency, often referred to as homodyne detection. This scheme

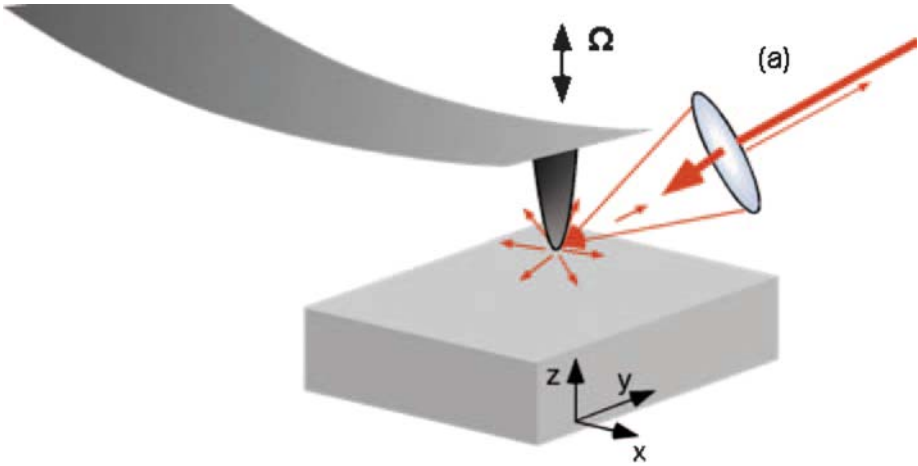


Figure 9 Basic experimental setup of a scattering-type near-field scanning optical microscope. The tip of an atomic force–microscope cantilever operating in tapping mode is illuminated by a focused laser (red arrow). Scattering from the tip is collected by a lens and detected at the tapping-mode frequency (Ω). Modified from Reference 78.

generally provides a high signal-to-noise ratio, and when recorded at the higher harmonics of tapping-mode frequency (74, 82, 83), it avoids complications associated with topographical-induced artifacts (26).

The reduction of the optical artifacts associated with nonlocalized optical interaction represents a significant improvement in the reliability and ease of interpretation of scattering NSOM measurements. Detecting at the higher harmonics of the modulation frequency takes advantage of the fact that the near-field scattering efficiency is highly nonlinear and generates harmonics as a function of tip-sample separation whereas the far-field scattering is largely linear and generates no harmonics (84). Figure 10 illustrates the effectiveness of this higher harmonic demodulation scheme in extracting the highly localized near fields from the extended far fields.

Homodyne-detection schemes have been used by numerous groups to study such diverse systems as DNA on surfaces (86), semiconducting nanostructures (87), polymer composites (33), and metallic nanostructures (88) with images demonstrating resolution better than 20 nm. An improvement on this basic scheme uses interferometric detection of the scattered field with a reference field to record the phase and amplitude of the scattered fields (84). Typically, the contrast in scattering NSOM is based on the intensity of the scattered radiation, E_{scatter} . This intensity is governed by the effective polarizability, α^{eff} , of the coupled probe-sample system: $E_{\text{scatter}} = \alpha^{\text{eff}} E$. As can be seen from Equation 1 above, the polarizability of the coupled tip-sample system is amplitude and phase dependent (α and β are complex). Thus, changes in the phase and amplitude of scattered

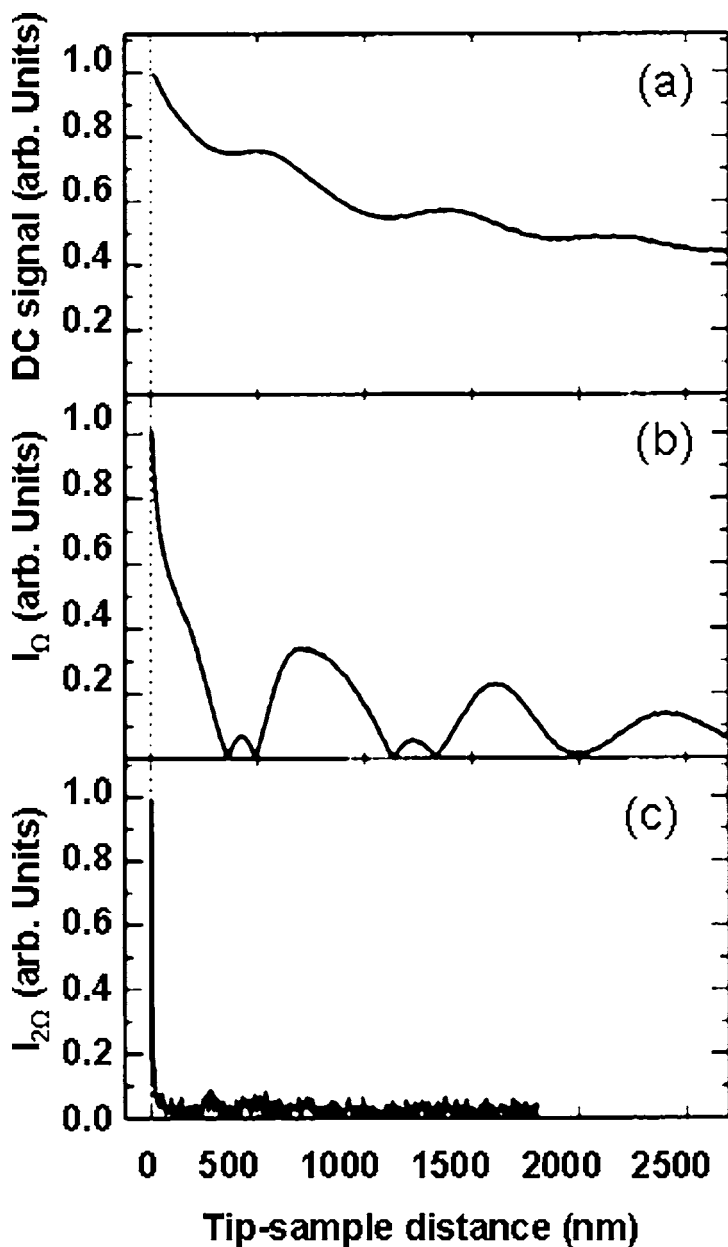


Figure 10 The optical signal amplitudes, DC signal (a), at the tapping-mode frequency (b) and at the second harmonic (c). At the second harmonic, the detected optical signal is highly localized at the surface, and nonlocalized scattering is virtually eliminated. From Reference 85.

radiation can be related to the complex dielectric constant of the local region of the sample surface, ϵ_{sample} : $\beta = (\epsilon_{\text{sample}} - 1)/(\epsilon_{\text{sample}} + 1)$. Thus, by acquiring the relative phase and amplitude shifts using interferometric-detection schemes in concert with scattering-type NSOM, one can measure or map out the nanometer-scale variations of heterogeneous materials. An illustration of this is shown in Figure 11.

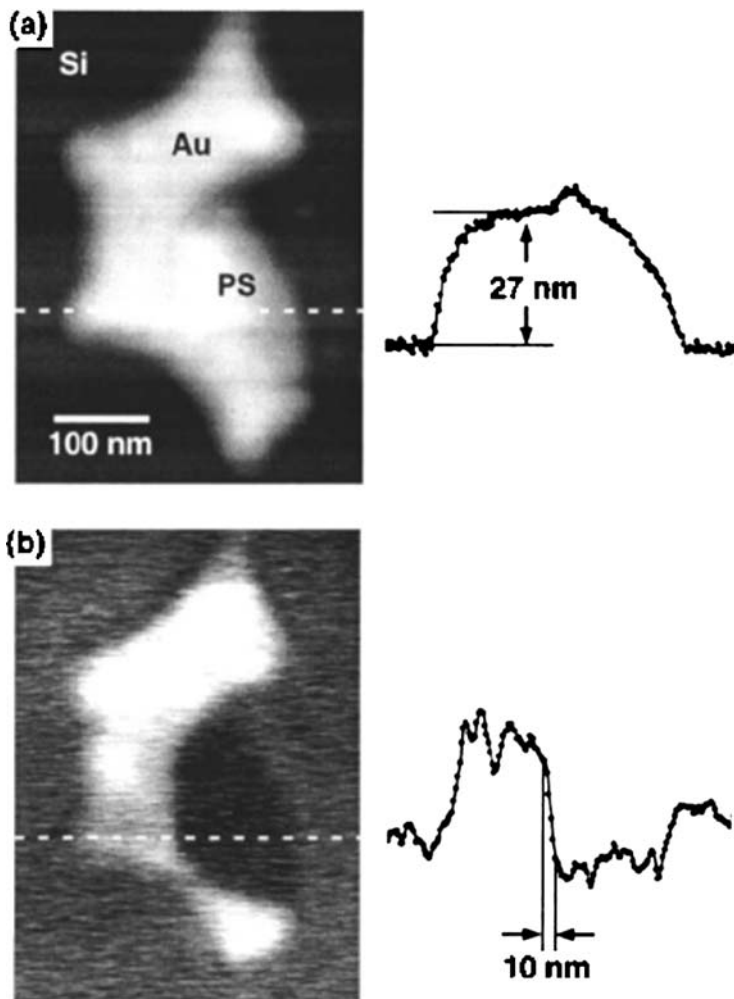


Figure 11 Scattering-type NSOM images of the topography (a) and the simultaneously recorded optical amplitude (b) of a three-component test sample comprised of gold (Au) and polystyrene (PS) nanostructures on silicon (Si). The accompanying line scans of the regions detailed by the dashed lines in the image illustrate both the attainable resolution and the ability to distinguish between the nanometer-scale components, Au and PS, of this system. From Reference 89.

Of importance in these images (recorded at 633 nm) is the unique ability of this detection scheme to contrast between different materials based on their dielectric properties at 633 nm. The measured values for the scattering amplitudes and phase are in good agreement with those predicted by various models (89).

With the achievable resolution of scattering NSOM below 10 nm, there is a need to increase the sensitivity or efficiency of the measured signal. This becomes increasingly important when the sample system is comprised of components with similar complex dielectric constants at a given wavelength. One method of increasing the signal efficiency is to move to regions in the spectrum containing resonances that further differentiate the materials comprising the sample or those taking advantage of resonances in the material-comprising tip. In the latter case, exploiting phonon resonances in common tip materials has shown to be a promising way to improve the efficiency and sensitivity of scattering-type NSOM (77). In the former case, whereas the refractive index of many polymers is essentially the same at visible wavelengths, the polymers vary substantially in the vibrational infrared as a result of absorption resonances giving rise to dispersive features in the refractive index via the Kramers-Kronig relations. An example of this is shown in Figure 12 where polystyrene inclusions are easily resolved in a

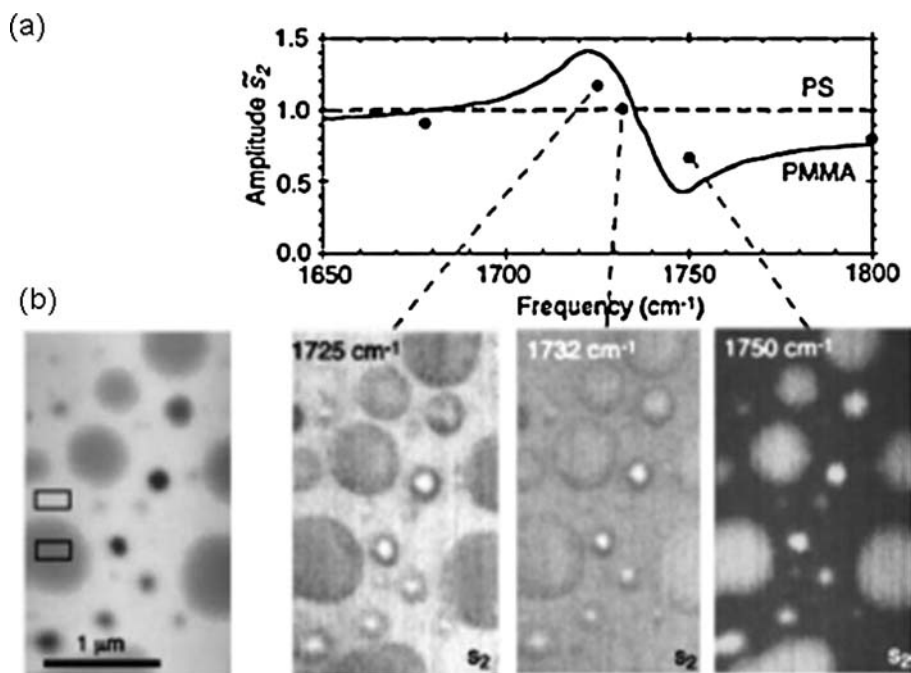


Figure 12 Infrared scattering-type NSOM contrast of polystyrene (PS) inclusions in a polymethylmetacrylate (PMMA). (a) The calculated and measured contrast as a function of wavelength. (b) Images of the topography (left) and recorded infrared amplitudes (right). From Reference 90.

polymethylmetacrylate continuum based on their refractive index in a vibrational infrared region where polymethylmetacrylate has a resonance and polystyrene does not. The power of this technique is evident. Operating a scattering near-field scanning optical microscope in this spectral region will allow identification of chemical species based on well-documented libraries of far-field infrared-absorption spectra with spatial resolution below 10 nm (90).

Whereas the results indicate the successful implementation of scattering NSOM, there are certain limitations to address before the full potential of this technique is realized, such as the inability to acquire information at frequencies other than the incident wavelength. This is a shortcoming that will be addressed by the technique in the section below.

LOCAL EXCITATION-BASED APPROACHES

The local-excitation scheme allows optical signals to be detected that are spectrally shifted from the excitation wavelength. In the past, this approach has been applied to two-photon excited fluorescence (24), single-photon excited fluorescence (47, 50, 80, 91), Raman scattering (25, 41–43), and CARS (44). To date, these experiments are performed with metal or semiconducting tips, but in the near future, other geometries with optimized resonant-antenna properties are likely to be employed (51–53).

The first high-resolution fluorescence images recorded with sharply pointed gold tips were demonstrated in 1999 (24). In these experiments, sample fluorescence was excited by two-photon absorption using the locally enhanced field at the tip apex. Fluorescence images with resolution exceeding 30 nm were demonstrated on photosynthetic membranes containing chlorophyll molecules as active fluorophores, and on J-aggregates consisting of strongly coupled pseudoisocyanine dye molecules. These initial experiments purposely made use of a nonlinear-optical interaction, such as two-photon absorption, to suppress background fluorescence associated with the direct irradiation of the sample surface (recall that the tip is irradiated in the far field). However, the advantage of nonlinear excitation of the sample was diminished by a background luminescence generated in the metal tip: Metals too are highly nonlinear optical materials. To increase the signal-to-noise ratio of near-field fluorescence imaging and to boost the sensitivity down to the single-molecule level, two other strategies have been put forth: (a) further reduction of the excitation volume and (b) modulation techniques similar to those employed in the scattering scheme discussed above. The first strategy was pursued and demonstrated by Guckenberger and coworkers (50, 92). In their approach a metal tip is directly fabricated on the end-face of a standard aperture probe (see Figure 13a). In this tip-on-aperture (TOA) approach, light emitted by the aperture directly couples to the tip and localizes the field at the tip's apex. This approach overcomes the problem of the far-field background associated with tip irradiation and therefore leads to a higher signal-to-background ratio. The tip of the TOA

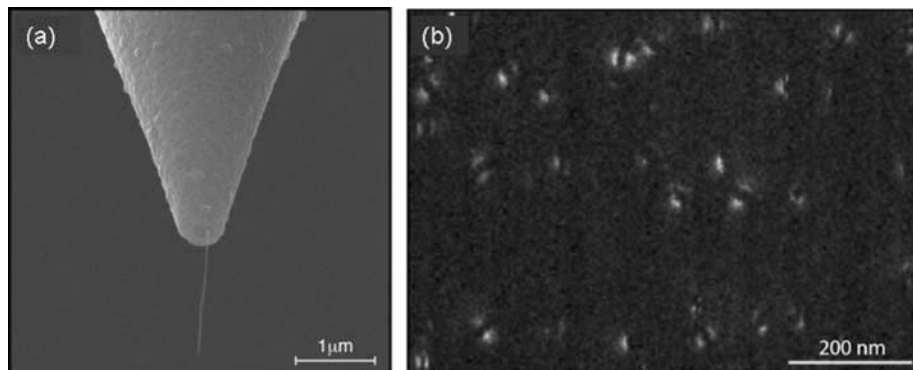


Figure 13 (a) Scanning electron microscopy image of a tip-on-aperture probe consisting of a SiO_x whisker grown directly on an aperture probe. (b) Fluorescence patterns of single molecules recorded with a tip-on-aperture probe. The centers of all molecules appear dark because of fluorescence quenching. From Reference 50.

probe shown in Figure 13a was fabricated by electron beam-assisted deposition of SiO_x . The tip was then cut to the desired length with a focused ion beam and overcoated with aluminum or gold.

Figure 13b shows fluorescence images of single molecules acquired with a TOA probe. Most molecules show up as a two-lobe pattern that results from the projection of the radially polarized electric field at the tip apex onto the dipole axis of the molecules. Interestingly, all fluorescence patterns exhibit a dark center, independent of the orientation of the molecular absorption dipole axis. This is an indication that fluorescence quenching becomes important for short tip-molecule distances (93, 94).

The tradeoff between fluorescence quenching and field enhancement is still being investigated. Different theoretical models have been developed (95–100), and experimental results are often inconsistent (47, 50, 80, 81, 91, 94, 101). This inconsistency originates from the fact that an excited molecule located near a metal structure (such as a tip) will relax to its ground state through radiative decay (γ_r) and nonradiative decay (γ_{nr}). In the presence of a pointed probe, both decay rates can be significantly increased over the free-space decay rate (γ_o) (100, 101). However, as long as γ_{nr} is much larger than γ_r , fluorescence will be quenched. For excitation intensities below saturation, the emitted fluorescence rate can be written as

$$\gamma_{em}(\omega) = \gamma_{exc}[1 - \gamma_{nr}/\gamma],$$

where $\gamma_{exc} \sim E^2$ is the excitation rate. The expression in the brackets corresponds to the apparent quantum yield $q_a = \gamma_r/\gamma$, $\gamma = \gamma_{nr} + \gamma_r$ represents the total decay rate. The individual rates γ_i depend on probe shape and material, and on the

molecule's orientation and distance from the tip. These rates need to be calculated computationally for a given tip-molecule configuration.

Gerton et al. (47) introduced the second approach for discriminating the background fluorescence associated with the direct irradiation of the sample surface. Here, they use a vertically oscillating tip similar to intermittent-mode (tapping-mode) AFM. If the locally emitted fluorescence were an analog signal, homodyne detection based on lock-in techniques would be a favorable strategy to boost the signal-to-noise ratio. However, fluorescence from a single quantum emitter is measured as a sequence of discrete events; hence a lock-in technique would not seem applicable. Nevertheless, this limitation can be overcome by a digital "time-stamping" filter (47) where the arrival times of single photons (or single spectra) are tagged with a time stamp from a clock. The periodic probe oscillation is also tagged with a time stamp, providing a phase reference for the optical data. The sets of time stamps can be saved to a memory for later analysis. The essence of this procedure is that only photons that fall into a predefined time window are detected. For example, only photons that arrive 5–10 μs after the probe reaches its nearest point to the sample surface are counted.

The local-excitation scheme has also been successfully combined with Raman scattering (25, 41–43). Here, the field enhancement at the laser-irradiated probe effectively increases the Raman scattering cross section of a molecule, similar to surface enhanced Raman scattering (102). Raman scattering probes the unique vibrational spectrum of the sample and directly reflects its chemical composition and molecular structure. Quenching as a result of the presence of a metal probe is absent in Raman scattering. Because Raman-scattered light is slightly spectrally shifted from the exciting radiation, the enhancement of the Raman-scattered light scales roughly with the fourth power of the electric field–enhancement factor, i.e., the excitation and emission pathways are enhanced roughly the same amount. The first near-field Raman images based on this approach have been reported for samples made of carbon nanotubes. Because of their nominally one-dimensional structure and their small size, carbon nanotubes are ideal test samples. A representative image recorded with near-field Raman microscopy is shown in Figure 14a. The contrast in the image corresponds to the strength of the G-line centered at $\nu = 1594 \text{ cm}^{-1}$. The spatial resolution of 15 nm is determined by the tip sharpness and the uniform signal along the nanotube. Furthermore, the weak D-band signal at $\nu \sim 1270 \text{ cm}^{-1}$ indicates that this chemical-vapor deposition grown tube is free of defects. It has been demonstrated that other growth methods can produce significant amounts of defects that can be localized and characterized with the near-field Raman technique (103). Figure 14c shows the signal enhancement as a function of tip-sample distance. This curve has been acquired for the G-line highlighted in Figure 14b. Considering the different areas probed by the near-field and far-field, an effective Raman enhancement factor of ~ 100 – 1000 is calculated, considerably lower than the theoretically predicted enhancement factors. It is also found that the enhancement is not uniform for the different spectral lines. Whereas near-field Raman scattering is likely to become a powerful technique for the characterization

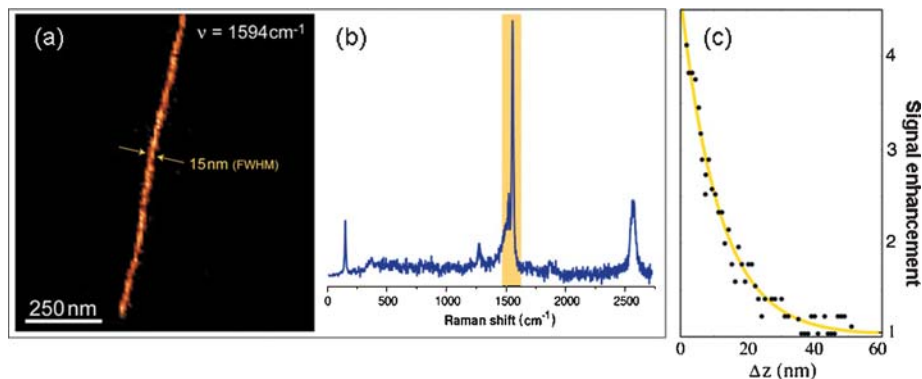


Figure 14 Near-field Raman imaging of single-walled carbon nanotubes (a). This image was recorded by raster-scanning the sample underneath a laser-irradiated metal tip and integrating, for each image pixel, the photon counts that fall into a narrow spectral bandwidth centered around the G-line at $\nu = 1594 \text{ cm}^{-1}$ (indicated by the *yellow stripe* in b). (b) Raman-scattering spectrum recorded on top of the nanotube. (c) Enhancement of the G-line signal as a function of tip-sample distance. The yellow line is an exponential fit with a 13-nm decay length.

of defects and dopants in nanotubes, the enhancement is currently too weak for applications in biology. Thus, future work must be aimed at optimizing the field enhancement by exploring finite-sized geometries inspired by classical antenna theory (51–53).

Near-field vibrational spectroscopy has recently been extended to the nonlinear regime by Kawata and coworkers (44). This group used near-field CARS to image clusters of DNA with contrast corresponding to the ring-breathing mode of diazole of adenine molecules. It can be expected that near-field CARS microscopy will find interesting applications in biological nanoscience similar to those currently studied by confocal CARS microscopy (104).

Metals are highly nonlinear-optical materials. Because of their small skin depth, the nonlinearity mainly enters through a nonlinear-surface susceptibility (105). Therefore, when a pointed metal probe is irradiated with laser pulses of a high peak intensity, different nonlinear-optical responses can be observed. The emitted spectrum shows peaks that can be assigned to second-harmonic generation, third-harmonic generation, sum-frequency generation, difference-frequency generation, and four-wave mixing. These spectral lines are generated by the enhanced field at the tip's apex; hence they constitute a highly confined photon source suitable for localized interactions with the sample surface. More importantly, the intensity of the spectral lines can be influenced by local electronic or vibrational sample resonances. This holds promise for the development of near-field extinction spectroscopy aimed at measuring the local polarizability of the sample.

CONCLUSION

Overall, research in the area of near-field microscopy and spectroscopy with pointed probes has produced promising results. It is evident that the local scattering and local excitation at a pointed probe holds promise for high-resolution chemical and materials characterization at finer length scales. As with other near-field methods, materials and sample systems with extended complexity in the z dimension complicate the straightforward analysis of NSOM images (85). This limits the present application of these techniques to thin-film samples with a thickness on the order of the near field, probe diameter, or to systems that are homogeneous in the z dimension. Other challenges reside in the development of improved probe structures and in the development of a physical understanding of the factors dictating the spectral response of complex, heterogeneous nanometer-scale systems.

ACKNOWLEDGMENTS

We acknowledge financial support from the U.S. Department of Energy (Grant DE-FG02-01ER15204) and from the Air Force Office for Scientific Research through the Multidisciplinary University Research Initiative (Grant F-49620-03-1-0379).

**The Annual Review of Physical Chemistry is online at
<http://physchem.annualreviews.org>**

LITERATURE CITED

- Pohl DW, Denk W, Lanz M. 1984. Optical stethoscopy: image recording with resolution $\lambda/20$. *Appl. Phys. Lett.* 44:651–53
- Lewis A, Isaacson M, Harootunian A, Muray A. 1984. Development of a 500-Å spatial-resolution light-microscope. *Ultramicroscopy* 13:227–31
- Dunn RC. 1999. Near-field scanning optical microscopy. *Chem. Rev.* 99:2891–927
- Paesler MA, Moyer PJ. 1996. *Near-Field Optics: Theory, Instrumentation, and Applications*. New York: Wiley Interscience
- Fillard JP. 1996. *Near-Field Optics and Nanoscopy*. Singapore: World Scientific
- Kawata S, Ohtsu M, Irie M. 2002. *Nano-Optics*. New York: Springer Verlag
- Prasad PN. 2004. *Nanophotonics*. New York: Wiley Interscience
- Courjon D. 2003. *Near Field Microscopy and Near Field Optics*. London: Imperial Coll. Press
- Richards D, Zayats A. 2004. Special issue on nano-optics and near field microscopy. *Philos. Trans. R. Soc. Lond. A* 362:699–919
- Rosner BT, van der Weide DW. 2002. High-frequency near-field microscopy. *Rev. Sci. Instrum.* 73:2505–25
- Syngé EH. 1928. A suggested methode for extending microscopic resolution into the ultra-microscopic region. *Philos. Mag.* 6:356–62
- Betzig E, Trautman JK. 1992. Near-field optics: microscopy, spectroscopy, and surface modification beyond the diffraction limit. *Science* 257:189–95
- Novotny L, Pohl DW. 1995. *Light Propagation in Scanning Near-Field Optical Microscopy*. Dordrecht: Kluwer Acad.
- Hecht B, Sick B, Wild UP, Deckert V, Zenobi R, et al. 2000. Scanning near-field optical microscopy with aperture probes:

- fundamentals and applications. *J. Chem. Phys.* 112:7761–74
15. La Rosa AH, Hallen HD. 2002. Compact method for optical induction of proximal probe heating and elongation. *Appl. Opt.* 41:2015–19
 16. Stahelin M, Bopp MA, Tarrach G, Meixner AJ, Zschokke-Granacher I. 1996. Temperature profile of fiber tips used in scanning near-field optical microscopy. *Appl. Phys. Lett.* 68:2603–5
 17. Inouye Y, Kawata S. 1994. Near-field scanning optical microscope with a metallic probe tip. *Opt. Lett.* 19:159–61
 18. Zenhausern F, Oboyle MP, Wickramasinghe HK. 1994. Apertureless near-field optical microscope. *Appl. Phys. Lett.* 65:1623–25
 19. Bachelot R, Gleyzes P, Boccard AC. 1995. Near-field optical microscope based on local perturbation of a diffraction spot. *Opt. Lett.* 20:1924–26
 20. Keilmann F, vanderWeide DW, Eickelkamp T, Merz R, Stockle D. 1996. Extreme sub-wavelength resolution with a scanning radio-frequency transmission microscope. *Opt. Commun.* 129:15–18
 21. Knoll B, Keilmann F. 1998. Scanning microscopy by mid-infrared near-field scattering. *Appl. Phys. A* 66:477–81
 22. Denk W, Pohl DW. 1991. Near-field optics: microscopy with nanometer-size fields. *J. Vac. Sci. Technol. B* 9:510–13
 23. Novotny L, Sanchez EJ, Xie XS. 1998. Near-field optical imaging using metal tips illuminated by higher-order Hermite-Gaussian beams. *Ultramicroscopy* 71:21–29
 24. Sanchez EJ, Novotny L, Xie XS. 1999. Near-field fluorescence microscopy based on two-photon excitation with metal tips. *Phys. Rev. Lett.* 82:4014–17
 25. Hartschuh A, Sanchez EJ, Xie XS, Novotny L. 2003. High-resolution near-field Raman microscopy of single-walled carbon nanotubes. *Phys. Rev. Lett.* 90:095503
 26. Hecht B, Bielefeldt H, Inouye Y, Pohl DW, Novotny L. 1997. Facts and artifacts in near-field optical microscopy. *J. Appl. Phys.* 81:2492–98
 27. Novotny L, Bian RX, Xie XS. 1997. Theory of nanometric optical tweezers. *Phys. Rev. Lett.* 79:645–48
 28. Martin OJF, Girard C. 1997. Controlling and tuning strong optical field gradients at a local probe microscope tip apex. *Appl. Phys. Lett.* 70:705–7
 29. McMullan D. 2002. The prehistory of scanned image microscopy. Part 1. Scanned optical microscopes. In *SPIE Milestone Series: Selected Papers on Near-Field Optics*, ed. S. Jutamulia, pp. 29–31. Bellingham, WA: SPIE
 30. Wessel J. 1985. Surface-enhanced optical microscopy. *J. Opt. Soc. Am. B* 2:1538–41
 31. Fischer UC, Pohl DW. 1989. Observation of single-particle plasmons by near-field optical microscopy. *Phys. Rev. Lett.* 62:458–61
 32. Bachelot R, Gleyzes P, Boccard AC. 1994. Near-field optical microscopy by local perturbation of a diffraction spot. *Microsc. Microanal. Microstruct.* 5:389–97
 33. Knoll B, Keilmann F. 1999. Near-field probing of vibrational absorption for chemical microscopy. *Nature* 399:134–37
 34. Keilmann F, Hillenbrand R. 2004. Near-field microscopy by elastic light scattering from a tip. *Philos. Trans. R. Soc. Lond. A* 362:787–805
 35. Decca RS, Drew HD, Empson KL. 1997. Investigation of the electric-field distribution at the subwavelength aperture of a near-field scanning optical microscope. *Appl. Phys. Lett.* 70:1932–34
 36. Betzig E, Chichester RJ. 1993. Single molecules observed by near-field scanning optical microscopy. *Science* 262:1422–25
 37. Veerman JA, Garcia-Parajo MF, Kuipers L, Van Hulst NF. 1999. Single molecule mapping of the optical field distribution of probes for near-field microscopy. *J. Microsc.* 194:477–82

38. Jersch J, Demming F, Dickman K. 1997. Nanostructuring with laser radiation in the nearfield of a tip from a scanning force microscope. *Appl. Phys. A* 64:29–32
39. Gorbunov AA, Pompe W. 1994. Thin-film nanoprocessing by laser STM combination. *Physica Status Solidi A* 145:333–38
40. Bragas AV, Landi SM, Martinez OE. 1998. Laser field enhancement at the scanning tunneling microscope junction measured by optical rectification. *Appl. Phys. Lett.* 72:2075–77
41. Stockle RM, Suh YD, Deckert V, Zenobi R. 2000. Nanoscale chemical analysis by tip-enhanced Raman spectroscopy. *Chem. Phys. Lett.* 318:131–36
42. Hayazawa N, Inouye Y, Sekkat Z, Kawata S. 2002. Near-field Raman imaging of organic molecules by an apertureless metallic probe scanning optical microscope. *J. Chem. Phys.* 117:1296–301
43. Anderson MS. 2000. Locally enhanced Raman spectroscopy with an atomic force microscope. *Appl. Phys. Lett.* 76:3130–32
44. Ichimura T, Hayazawa N, Hashimoto M, Inouye Y, Kawata S. 2004. Tip-enhanced coherent anti-Stokes Raman scattering for vibrational nanoimaging. *Phys. Rev. Lett.* 92:220801
45. Bohn JL, Nesbitt DJ, Gallagher A. 2001. Field enhancement in apertureless near-field scanning optical microscopy. *J. Opt. Soc. Am. A* 18:2998–3006
46. Hamann HF, Larbadi M, Barzen S, Brown T, Gallagher A, Nesbitt DJ. 2003. Extinction near-field optical microscopy. *Opt. Commun.* 227:1–13
47. Gerton JM, Wade LA, Lessard GA, Ma Z, Quake SR. 2004. Tip-enhanced fluorescence microscopy at 10 nanometer resolution. *Phys. Rev. Lett.* 93:180801
48. Zenhausern F, Martin Y, Wickramasinghe HK. 1995. Scanning interferometric apertureless microscopy: optical imaging at 10 Angstrom resolution. *Science* 269:1083–85
49. Haefliger D, Plitzko JM, Hillenbrand R. 2004. Contrast and scattering efficiency of scattering-type near-field optical probes. *Appl. Phys. Lett.* 85:4466–68
50. Frey HG, Witt S, Felderer K, Guckenberger R. 2004. High-resolution imaging of single fluorescent molecules with the optical near-field of a metal tip. *Phys. Rev. Lett.* 93:200801
51. Muhlschlegel P, Eisler HJ, Martin OJF, Hecht B, Pohl DW. 2005. Resonant optical antennas. *Science* 308:1607–9
52. Schuck PJ, Fromm DP, Sundaramurthy A, Kino GS, Moerner WE. 2005. Improving the mismatch between light and nanoscale objects with gold bowtie nanoantennas. *Phys. Rev. Lett.* 94:017402
53. Grober RD, Schoelkopf RJ, Prober DE. 1997. Optical antenna: towards a unity efficiency near-field optical probe. *Appl. Phys. Lett.* 70:1354
54. Farahani JN, Pohl DW, Eisler HJ, Hecht B. 2005. Single quantum dot coupled to a scanning optical antenna: a tunable superemitter. *Phys. Rev. Lett.* 95:017402
55. Calander N, Willander M. 2002. Theory of surface-plasmon resonance optical-field enhancement at prolate spheroids. *J. Appl. Phys.* 92:4878–84
56. Martin YC, Hamann HF, Wickramasinghe HK. 2001. Strength of the electric field in apertureless near-field optical microscopy. *J. Appl. Phys.* 89:5774–78
57. Krug JT, Sanchez EJ, Xie XS. 2002. Design of near-field optical probes with optimal field enhancement by finite difference time domain electromagnetic simulation. *J. Chem. Phys.* 116:10895–901
58. Kottmann JP, Martin OJF, Smith DR, Schultz S. 2001. Dramatic localized electromagnetic enhancement in plasmon resonant nanowires. *Chem. Phys. Lett.* 341:1–6
59. Sonnichsen C, Franzl T, Wilk T, von Plessen G, Feldmann J, et al. 2002. Dramatic reduction of plasmon damping in gold nanorods. *Phys. Rev. Lett.* 88:077402
60. Jin RC, Cao YW, Mirkin CA, Kelly KL,

- Schatz GC, Zheng JG. 2001. Photoinduced conversion of silver nanospheres to nanoprisms. *Science* 294:1901–3
61. Mock JJ, Barbic M, Smith DR, Schultz DA, Schultz S. 2002. Shape effects in plasmon resonance of individual colloidal silver nanoparticles. *J. Chem. Phys.* 116:6755–59
62. Gole A, Murphy CJ. 2004. Seed-mediated synthesis of gold nanorods: role of the size and nature of the seed. *Chem. Mater.* 16:3633–40
63. Kalkbrenner T, Ramstein M, Mlynek J, Sandoghdar V. 2001. A single gold particle as a probe for apertureless scanning near-field optical microscopy. *J. Microsc.* 202:72–76
64. Renger J, Grafstrom S, Eng LM, Deckert V. 2004. Evanescent wave scattering and local electric field enhancement at ellipsoidal silver particles in the vicinity of a glass surface. *J. Optic. Soc. Am. A* 21:1362–67
65. Neacsu CC, Steudle GA, Raschko MB. 2005. Plasmonic light scattering from nanoscopic metal tips. *Appl. Phys. B* 80:295–300
66. Kawata Y, Xu C, Denk W. 1999. Feasibility of molecular-resolution fluorescence near-field microscopy using multiphoton absorption and field enhancement near a sharp tip. *J. Appl. Phys.* 85:1294–301
67. Zayats AV. 1999. Electromagnetic field enhancement in the context of apertureless near-field microscopy. *Opt. Commun.* 161:156–62
68. Bouhelier A, Renger J, Beversluis MR, Novotny L. 2003. Plasmon-coupled tip-enhanced near-field optical microscopy. *J. Microsc.* 210:220–24
69. Kreibig U, Bour G, Hilger A, Gartz M. 1999. Optical properties of cluster-matter: influences of interfaces. *Physica Status Solidi A* 175:351–66
70. Mukamel S. 1995. *Principles of Nonlinear Optical Spectroscopy*. New York: Oxford Univ. Press
71. Georges AT. 2001. Calculation of surface electromagnetic fields in laser-metal surface interaction. *Opt. Commun.* 188:321–31
72. Bouhelier A, Beversluis M, Hartschuh A, Novotny L. 2003. Near-field second-harmonic generation induced by local field enhancement. *Phys. Rev. Lett.* 90:013903
73. Hafner C. 1990. *The Generalized Multiple Multipole Technique for Computational Electromagnetics*. Boston: Artech
74. Labardi M, Allegrini M, Zavelani-Rossi M, Polli D, Cerullo G, et al. 2004. Highly efficient second-harmonic nanosource for near-field optics and microscopy. *Opt. Lett.* 29:62–64
75. Beversluis MR, Bouhelier A, Novotny L. 2003. Continuum generation from single gold nanostructures through near-field mediated intraband transitions. *Phys. Rev. B* 68:115433
76. Hillenbrand R, Knoll B, Keilmann F. 2001. Pure optical contrast in scattering-type scanning near-field microscopy. *J. Microsc.* 202:77–83
77. Hillenbrand R, Taubner T, Keilmann F. 2002. Phonon-enhanced light-matter interaction at the nanometre scale. *Nature* 418:159–62
78. Keilmann F. 2004. Scattering-type near-field optical microscopy. *J. Electron Microsc.* 53:187–92
79. Gersten J, Nitzan A. 1980. Electromagnetic theory of enhanced Raman scattering by molecules adsorbed on rough surfaces. *J. Chem. Phys.* 73:3023–37
80. Hamann HF, Gallagher A, Nesbitt DJ. 2000. Near-field fluorescence imaging by localized field enhancement near a sharp probe tip. *Appl. Phys. Lett.* 76:1953–55
81. Azoulay J, Debarre A, Richard A, Tchenio P. 1999. Field enhancement and apertureless near-field optical spectroscopy of single molecules. *J. Microsc.* 194:486–90

82. Hillenbrand R, Stark M, Guckenberger R. 2000. Higher-harmonics generation in tapping-mode atomic-force microscopy: insights into the tip-sample interaction. *Appl. Phys. Lett.* 76:3478–80
83. Wurtz G, Bachelot R, Royer P. 1999. Imaging a GaAlAs laser diode in operation using apertureless scanning near-field optical microscopy. *Eur. Phys. J. Appl. Phys.* 5:269–75
84. Hillenbrand R, Keilmann F. 2000. Complex optical constants on a subwavelength scale. *Phys. Rev. Lett.* 85:3029–32
85. Raschke MB, Lienau C. 2003. Apertureless near-field optical microscopy: tip-sample coupling in elastic light scattering. *Appl. Phys. Lett.* 83:5089–91
86. Akhremitchev BB, Sun YJ, Stebounova L, Walker GC. 2002. Monolayer-sensitive infrared imaging of DNA stripes using apertureless near-field microscopy. *Langmuir* 18:5325–28
87. Kim ZH, Liu B, Leone SR. 2005. Nanometer-scale optical imaging of epitaxially grown GaN and InN islands using apertureless near-field microscopy. *J. Phys. Chem. B* 109:8503–8
88. Hamann HF, Gallagher A, Nesbitt DJ. 1998. Enhanced sensitivity near-field scanning optical microscopy at high spatial resolution. *Appl. Phys. Lett.* 73:1469–71
89. Hillenbrand R, Keilmann F. 2002. Material-specific mapping of metal/semiconductor/dielectric nanosystems at 10 nm resolution by backscattering near-field optical microscopy. *Appl. Phys. Lett.* 80:25–27
90. Taubner T, Hillenbrand R, Keilmann F. 2004. Nanoscale polymer recognition by spectral signature in scattering infrared near-field microscopy. *Appl. Phys. Lett.* 85:5064–66
91. Kramer A, Trabesinger W, Hecht B, Wild UP. 2002. Optical near-field enhancement at a metal tip probed by a single fluorophore. *Appl. Phys. Lett.* 80:1652–54
92. Frey HG, Keilmann F, Kriele A, Guckenberger R. 2002. Enhancing the resolution of scanning near-field optical microscopy by a metal tip grown on an aperture probe. *Appl. Phys. Lett.* 81:5030–32
93. Chance RR, Miller AH, Prock A, Silbey R. 1975. Fluorescence and energy-transfer near interfaces: complete and quantitative description of Eu + 3-mirror systems. *J. Chem. Phys.* 63:1589–95
94. Trabesinger W, Kramer A, Kreiter M, Hecht B, Wild UP. 2002. Single-molecule near-field optical energy transfer microscopy. *Appl. Phys. Lett.* 81:2118–20
95. des Francs GC, Girard C. 2002. Theory of near-field optical imaging with a single fluorescent molecule used as a point-like detector. *Chem. Phys.* 282:277–87
96. Girard C, Martin OJF, Dereux A. 1995. Molecular lifetime changes induced by nanometer-scale optical-fields. *Phys. Rev. Lett.* 75:3098–101
97. Azoulay J, Debarre A, Richard A, Tchenio P. 2000. Quenching and enhancement of single-molecule fluorescence under metallic and dielectric tips. *Europhys. Lett.* 51:374–80
98. Thomas M, Greffet JJ, Carminati R, Arias-Gonzalez JR. 2004. Single-molecule spontaneous emission close to absorbing nanostructures. *Appl. Phys. Lett.* 85:3863–65
99. Krug JT, Sanchez EJ, Xie XS. 2005. Fluorescence quenching in tip-enhanced nonlinear optical microscopy. *Appl. Phys. Lett.* 86:233102
100. Novotny L. 1996. Single molecule fluorescence in inhomogeneous environments. *Appl. Phys. Lett.* 69:3806–8
101. Barnes WL. 1998. Fluorescence near interfaces: the role of photonic mode density. *J. Mod. Opt.* 45:661–99
102. Otto A, Mrozek I, Grabhorn H, Akemann W. 1992. Surface-enhanced Raman-scattering. *J. Phys. Condens. Matter* 4:1143–212
103. Anderson N, Hartschuh A, Cronin S,

- Novotny L. 2005. Nanoscale vibrational analysis of single-walled carbon nanotubes. *J. Am. Chem. Soc.* 127:2533–37
104. Zumbusch A, Holtom GR, Xie XS. 1999. Three-dimensional vibrational imaging by coherent anti-Stokes Raman scattering. *Phys. Rev. Lett.* 82:4142–45
105. Guyot-Sionnest P, Shen YR. 1987. Local and nonlocal surface nonlinearities for surface optical 2nd-harmonic generation. *Phys. Rev. B* 35:4420–66